

Bidimensional dynamic maps in optical resonators

V. Aboites^a, Y. Barmenkov^a, A. Kiryanov^a and M. Wilson^b

^a*Centro de Investigaciones en Óptica,
Loma del Bosque 115, León, 37150 México.*

e-mail: aboites@cio.mx

^b*Université des Sciences et Technologies de Lille 1,
CNRS UMR 8523-UFR de Physique-Bâtiment P5, 59655 Villeneuve d'Ascq Cedex, France.*

Received 29 August 2012; accepted 24 February 2014

In this article an introduction to the dynamical behavior of a beam within a ring phase-conjugated optical resonator is presented and modeled using two dimensional iterative maps. Three well known iterative maps are described: Duffing, Tinkerbell and Hénon, and are applied to the description of optical resonators. It is explicitly shown how the difference equations of these maps can be used to describe the dynamic behavior of what we call Tinkerbell, Duffing and Hénon beams *i.e.* beams that behave according to these maps. The matrix of a map generating device are found in terms of the specific map parameters, the state variables and the resonator parameters for each of the three named maps.

Keywords: Resonator; chaotic maps; phase conjugation.

En este artículo se presenta una introducción al comportamiento dinámico de un haz dentro de un resonador óptico de anillo de conjugación de fase el cual es modelado usando mapas iterativos bidimensionales. Tres bien conocidos mapas iterativos son descritos: Duffing, Tinkerbell y Hénon, y son utilizados para la descripción de resonadores ópticos. Se muestra explícitamente cómo las ecuaciones de diferencia de los mapeos anteriores pueden ser utilizados para describir el comportamiento dinámico de lo que llamamos, haces de Tinkerbell, Duffing y Hénon *i.e.* haces que se comportan siguiendo dichos mapas. La matriz de un dispositivo generador del mapeo se encuentra en términos de los parámetros específicos del mapa, de las variables de estado y de los parámetros del resonador para cada uno de los tres mapas anteriores.

Descriptores: Resonador; mapeo caótico; resonador de anillo.

PACS: 42.15.-I; 42.60.Da; 42.65.Hw

1. Introduction

Recently, optical phase conjugation (OPC) has been an important research subject in the field of lasers and nonlinear optics. As it is known, OPC defines a link between two coherent optical beams propagating in opposite directions with reversed wave front and identical transverse amplitude distributions. The unique characteristic of a pair of phase-conjugate beams is that the aberration influence imposed on the forward beam passed through an inhomogeneous or disturbing medium can be automatically removed for the backward beam passed through the same disturbing medium. There are three leading approaches that are efficiently able to generate the backward phase-conjugate beam. The first one is based on the degenerate (or partially degenerate) four-wave mixing processes (FWM), the second is based on a variety of backward simulated (*e.g.* Brillouin, Raman or Kerr) scattering processes, and the third is based on one-photon or multi-photon pumped backward stimulated emission (lasing) processes. Among these different methods, there is a common physical mechanism in generating a backward phase-conjugate beam, which is the formation of the induced holographic grating and the subsequent wave-front restoration via a backward reading beam. In most experimental studies, certain types of resonance enhancements of induced refractive-index changes are desirable for obtaining higher grating-refraction efficiency. OPC-associated techniques can be effectively utilized in many different applica-

tion areas: such as high-brightness laser oscillator/amplifier systems, cavity-less lasing devices, laser target-aiming systems, aberration correction for coherent-light transmission and reflection through disturbing media, long distance optical fiber communications with ultra-high bit-rate, optical phase locking and coupling systems, and novel optical data storage and processing systems (see Ref. 1 and references therein). The power performance of a phase conjugated laser oscillator can be significantly improved introducing intracavity nonlinear elements, *e.g.* Eichler *et al.*, [2] and O'Connor *et al.*, [3] showed that a stimulated-Brillouin-scattering (SBS) phase conjugating cell placed inside the resonator of a solid-state laser reduces its optical coherence length, because each axial mode of the phase conjugated oscillator experiences a frequency shift at every reflection by the SBS cell resulting in a multi-frequency lasing spectrum, that makes the laser insensitive to changing operating conditions such as pulse repetition frequency, pump energy, etc. This capacity is very important for many laser applications including ranging and remote sensing. The intracavity cell is also able to compensate optical aberrations from the resonator and from thermal effects in the active medium, resulting in near diffraction limited output [4], and eliminate the need for a conventional Q-switch as well, because its intensity-dependent reflectivity acts as a passive Q-switch, typically producing a train of nanosecond pulses of diffraction limited beam quality. One more significant use of OPC is a so-called short hologram,

which does not exhibit in-depth diffraction deformation of the fine speckle pattern of the recording fields [5]. A thermal hologram in the output mirror was recorded by two speckle waves produced as a result of this recording a ring Nd:YAG laser [6]. Phase conjugation by SBS represents a fundamentally encouraging approach for achieving power scaling of solid-state lasers [7,8] and optical fibers [9]. There are several theoretical models to describe OPC in resonators and lasers. One of them is to use the SBS reflection as one of the cavity mirrors of a laser resonator to form a so-called linear phase conjugate resonator [10], however ring-phase conjugate resonators are also possible [11]. The theoretical model of an OPC laser in transient operation [12] considers the temporal and spatial dynamic of the input field the Stokes field and the acoustic-wave amplitude in the SBS cell. On the other hand the spatial mode analysis of a laser may be carried out using transfer matrices, also know as ABCD matrices, which are a useful mathematical tool when studying the propagation of light rays through complex optical systems. They provide a simple way to obtain the final key characteristics (position and angle) of the ray. As an important example we could mention that transfer matrices have been used to study self-adaptive laser resonators where the laser oscillator is made out of a plane output coupler and an infinite nonlinear FWM medium in a self-intersecting loop geometry [13].

In this article we put forward an approach where the intracavity element is presented in the context of an iterative map (*e.g.* Tinkerbell, Duffing and Hénon) whose state is determined by its previous state. It is shown that the behavior of a beam within a ring optical resonator may be well described by a particular iterative map and the necessary conditions for its occurrence are discussed. In particular, it is shown that the introduction of a specific element within a ring phase-conjugated resonator may produce beams described by a Duffing, Tinkerbell or Hénon map, which we call “Tinkerbell, Duffing or Hénon beams”.

The idea of introducing map generating elements in optical resonators from a mathematical viewpoint was originally explored in [14-17] and due to its pedagogical purposes this paper is based on those results.

This article is organized as follows: Sec. 2 provides an introduction to discuss the matrix optics elements on which this work is based. Section 3 presents some of the basic features of iterative maps, in particular of the Tinkerbell, Duffing and Hénon maps, Secs. 4, 5 and 6 shows, each one of them, the main characteristics of the map generation matrix and Tinkerbell, Duffing and Hénon Beams, as well as the general case for each beams in a ring phase conjugated resonator. Finally Sec. 6 presents the conclusions.

2. ABCD Matrix Optics

As it is known, any optical element may be described by a 2×2 matrix in paraxial optics. Assuming cylindrical symmetry around the optical axis, and defining at a given position z both the perpendicular distance of any ray to the optical axis

and its angle with the same axis as $y(z)$ and $\theta(z)$, when the ray undergoes a transformation as it travels through an optical system represented by the matrix $[A, B, C, D]$, the resultant values of y and θ are given by [18]:

$$\begin{pmatrix} y_{n+1} \\ \theta_{n+1} \end{pmatrix} = \begin{pmatrix} A & B \\ C & D \end{pmatrix} \begin{pmatrix} y_n \\ \theta_n \end{pmatrix}. \quad (1)$$

For any optical system, one may obtain the total $[A, B, C, D]$ matrix, by carrying out the matrix product of the matrices describing each one of the optical elements in the system.

Constant ABCD elements

In passive optical elements, such as lenses, interfaces between two media, reflections, propagation, and many others, the elements A, B, C, D are constants and the determinant $\text{Det}[A, B, C, D] = n_n/n_{n+1}$, where n_n and n_{n+1} are the refraction index before and after the optical element described by the matrix. Since typically n_n and n_{n+1} are the same, it holds that $\text{Det}[A, B, C, D] = 1$.

Non constant ABCD elements

Nevertheless, for active or non-linear optical elements the A, B, C, D matrix elements are not constant but may be functions of various parameters. The following three examples are worth mentioning.

Curved interface with a Kerr electro-optic material

Due to the electro-optic Kerr effect the refraction index of an optical media n is a function of the electric field strength E [19]. The change of the refraction index is given by $\Delta n = \lambda K E^2$, where λ is the wavelength and K is the Kerr constant of the media. For example, the $[A, B, C, D]$ matrix of a curved surface of radius of curvature r separating two regions of refractive index n_1 and n_2 (taking the center of the radius of curvature positive to the right in the zone of refractive index n_2) is given as

$$\begin{pmatrix} 1 & 0 \\ -\frac{(n_2 - n_1)}{r} & 1 \end{pmatrix}. \quad (2)$$

Having vacuum ($n_1 = 1$) on the left of the interface and a Kerr electro-optic material on the right. The above $[ABCD]$ matrix becomes

$$\begin{pmatrix} 1 & 0 \\ -\frac{(n_2(E) - 1)}{r} & 1 \end{pmatrix}. \quad (3)$$

Clearly the elements A, B, D are constants but element C is a function of the electric field E .

Phase conjugate mirror

A second example is a phase conjugate mirror. The process of phase conjugation has the property of retracing an incoming ray along the same incident path [7]. The ideal $ABCD$ phase conjugate matrix is

$$\begin{pmatrix} 1 & 0 \\ 0 & -1 \end{pmatrix}. \tag{4}$$

One may notice that the determinant of this particular matrix is not 1 but -1. The $ABCD$ matrix of a real phase conjugated mirror must take into account the specific process to produce the phase conjugation. As already mentioned, typically phase conjugation is achieved in two ways; Four Wave Mixing or using a stimulated scattering process such as Brillouin, *i.e.* Stimulated Brillouin Scattering (SBS). However upon reflection on a stimulated SBS phase conjugated mirror, the reflected wave has its frequency ω downshifted to $\omega - \delta = \omega(1 - \delta/\omega)$ where δ is the characteristic Brillouin downshift frequency of the mirror material (typically $\delta/\omega \ll 1$). In a non-ideal (*i.e.* real) case one must take the downshifting frequency into account and the $ABCD$ matrix reads

$$\begin{pmatrix} 1 - \frac{\delta}{\omega} & 0 \\ 0 & -1 \end{pmatrix}. \tag{5}$$

Furthermore, since in phase conjugation by SBS a light intensity threshold must be reached in order to have an exponential amplification of the scattered light, the above ideal matrix (4) must be modified. The scattered light intensity at position z in the medium is given as

$$I_S(z) = I_S(0) \exp(g_B I_L l), \tag{6}$$

where $I_S(0)$ is the initial level of scattering, g_B denotes the characteristic exponential gain coefficient of the scattering process, I_L is the intensity of the incident light beam, and l is the interaction length over which amplification takes place. Given the amplification $G = \exp(g_B(\nu)I_L l)$ the threshold gain factor is commonly taken as $G \sim \exp(30) \approx 10^{13}$ which corresponds to a threshold intensity

$$I_{L,th} = \frac{30}{g_B l}. \tag{7}$$

The modeling of a real stimulated Brillouin scattering phase conjugate mirror usually takes into account a Gaussian aperture of radius a at intensity $1/e^2$ placed before an ideal phase conjugator. In this way the reflected beam is Gaussian and only the parts of the Gaussian incident beam with intensity above threshold are phase conjugate reflected. The matrix of this aperture is given by:

$$\begin{pmatrix} 1 & 0 \\ -\frac{i\lambda}{\pi a^2} & 1 \end{pmatrix}, \tag{8}$$

where the aperture a is a function of the incident light intensity $a(I_L)$ (I_L must reach threshold to initiate the scattering process). As we can see, depending on the model, the $ABCD$ matrix elements of a phase conjugated mirror may depend on several parameters such as the Brillouin downshifting frequency, the Gaussian aperture radius and the incident light intensity [20].

Systems with hysteresis

At last, as third example we may consider a system with hysteresis. It is well known that such systems exhibit memory. There are many examples of materials with electric, magnetic and elastic hysteresis, as well as systems in neuroscience, biology, electronics, energy and even economics which show hysteresis. As it is known in a system with no hysteresis, it is possible to predict the system's output at an instant in time given only its input at that instant in time. However in a system with hysteresis, this is not possible; there is no way to predict the output without knowing the system's previous state and there is no way to know the system's state without looking at the history of the input. This means that it is necessary to know the path that the input followed before it reached its current value [21]. For an optical element with hysteresis the $ABCD$ matrix elements are function of the $y_n, y_{n-1}, \dots, y_{n-i}$ and $\theta_n, \theta_{n-1}, \dots, \theta_{n-i}$ and its knowledge is necessary in order to find the state y_{n+1}, θ_{n+1} . In general, taking into account hysteresis, the $[A, B, C, D]$ matrix of Eq. (1) may be written as

$$\begin{pmatrix} A & B \\ C & D \end{pmatrix} = \begin{pmatrix} A(y_n, y_{n-1}, \dots, y_{n-i}, \theta_n, \theta_{n-1}, \dots, \theta_{n-i}) & B(y_n, y_{n-1}, \dots, y_{n-i}, \theta_n, \theta_{n-1}, \dots, \theta_{n-i}) \\ C(y_n, y_{n-1}, \dots, y_{n-i}, \theta_n, \theta_{n-1}, \dots, \theta_{n-i}) & D(y_n, y_{n-1}, \dots, y_{n-i}, \theta_n, \theta_{n-1}, \dots, \theta_{n-i}) \end{pmatrix}. \tag{9}$$

3. Dynamic Maps

An extensive list of two-dimensional maps may be found in Ref. 22. A few examples are Tinkerbell, Duffing and Hénon maps. As will be shown next they may be written as a matrix dynamical system such as the one described by Eq. (1) or equivalently as

$$y_{n+1} = Ay_n + B\theta_n, \tag{10a}$$

$$\theta_{n+1} = Cy_n + D\theta_n. \tag{10b}$$

Tinkerbell Map

The Tinkerbell map [23,24] is a discrete-time dynamical system given by the equations:

$$y_{n+1} = y_n^2 - \theta_n^2 + \alpha y_n + \beta \theta_n, \tag{11a}$$

$$\theta_{n+1} = 2y_n\theta_n + \gamma y_n + \delta\theta_n, \tag{11b}$$

where y_n and θ_n are the scalar state variables and $\alpha, \beta, \gamma,$ and δ the map parameters. In order to write the Tinkerbell map as a matrix system such as Eq. (1) the following values for the coefficients A, B, C and D must hold

$$A(y_n, \alpha) = y_n + \alpha, \tag{12}$$

$$B(\theta_n, \beta) = -\theta_n + \beta, \tag{13}$$

$$C(\theta_n, \gamma) = 2\theta_n + \gamma, \tag{14}$$

$$D(\delta) = \delta. \tag{15}$$

It should be noted that these coefficients are not constants but depend on the state variables y_n and θ_n and the Tinkerbell map parameters $\alpha, \beta, \gamma,$ and δ . Therefore as an $ABCD$ matrix system the Tinkerbell map may be written as,

$$\begin{pmatrix} y_{n+1} \\ \theta_{n+1} \end{pmatrix} = \begin{pmatrix} y_n + \alpha & -\theta_n + \beta \\ 2\theta_n + \gamma & \delta \end{pmatrix} \begin{pmatrix} y_n \\ \theta_n \end{pmatrix}. \tag{16}$$

Hénon Map

The Hénon map has been widely studied due to its nonlinear chaotic dynamics. Hénon map is a popular example of a two-dimensional quadratic mapping which produces a discrete-time system with chaotic behavior. The Hénon map is described by the following two difference equations [25,26]

$$y_{n+1} = 1 - \alpha y_n^2 + \theta_n, \tag{17a}$$

$$\theta_{n+1} = \beta y_n. \tag{17b}$$

Following similar steps as those of the Tinkerbell map, this map may be written as a dynamic matrix system

$$\begin{pmatrix} y_{n+1} \\ \theta_{n+1} \end{pmatrix} = \begin{pmatrix} \frac{1}{y_n} - \alpha y_n & 1 \\ \beta & 0 \end{pmatrix} \begin{pmatrix} y_n \\ \theta_n \end{pmatrix}, \tag{18}$$

where y_n and θ_n are the scalar state variables which can be measured as time series and α and β the map parameters. In many control systems α is a control parameter. The Jacobian β ($0 \leq \beta \leq 1$) is related to dissipation. The dynamics of the Hénon map is well studied (see, for instance, Ref. 27) and its fixed points are given by:

$$(y_1, \theta_1) = \left(\frac{-\beta - 1 + \sqrt{(\beta + 1)^2 + 4\alpha}}{2\alpha}, -\beta y_1 \right), \tag{19}$$

$$(y_2, \theta_2) = \left(\frac{-\beta - 1 - \sqrt{(\beta + 1)^2 + 4\alpha}}{2\alpha}, -\beta y_2 \right), \tag{20}$$

and the corresponding eigenvalues are

$$\lambda_{1,2} = -\alpha y \pm \sqrt{(\alpha y)^2 - \beta}. \tag{21}$$

Duffing Map

The study of the stability and chaos of the Duffing map has been the topic of many articles [28-29]. The Duffing map is a dynamical system which may be written as follows:

$$y_{n+1} = \theta_n, \tag{22a}$$

$$\theta_{n+1} = -\beta y_n + \alpha \theta_n - \theta_n^3 \tag{22b}$$

where y_n and θ_n are the scalar state variables and α and β the map parameters. In order to write the Duffing map equations as a matrix system Eq. (1) the following values for the coefficients A, B, C and D must hold. It should be noted that these coefficients are not constants but depend on θ_n and the Duffing map parameters are as follows:

$$A = 0 \tag{23}$$

$$B = 1 \tag{24}$$

$$C(\beta) = -\beta \tag{25}$$

$$D(\theta_n, \alpha) = \alpha - \theta_n^2. \tag{26}$$

Therefore as an ABCD matrix system the Duffing map may be written as

$$\begin{pmatrix} y_{n+1} \\ \theta_{n+1} \end{pmatrix} = \begin{pmatrix} 0 & 1 \\ -\beta & \alpha - \theta_n^2 \end{pmatrix} \begin{pmatrix} y_n \\ \theta_n \end{pmatrix}. \tag{27}$$

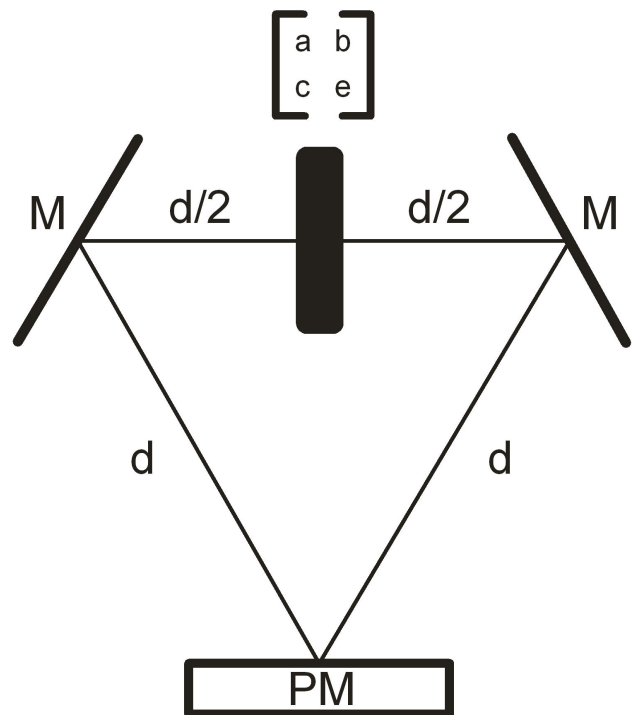


FIGURE 1. Ring phase conjugated laser resonator with chaos generating element.

4. Maps in a ring phase-conjugated resonator

In this section an optical resonator with a specific map behavior for the variables y and θ is presented. Figure 1 shows a ring phase-conjugated resonator consisting of two ideal mirrors, an ideal phase conjugate mirror and a yet unknown optical element described by a matrix $[a, b, c, e]$. The two perfect plain mirrors [M] and the ideal phase conjugated mirror [PM] are separated by a distance d . The matrices involved in this resonator are: the identity matrix: $\begin{pmatrix} 1 & 0 \\ 0 & 1 \end{pmatrix}$ for the plane mirrors [M], $\begin{pmatrix} 1 & 0 \\ 0 & -1 \end{pmatrix}$ for the ideal phase conjugated mirror [PM], $\begin{pmatrix} 1 & d \\ 0 & 1 \end{pmatrix}$ for a distance d translation and, in addition, the unknown map generating device matrix represented by $\begin{pmatrix} a & b \\ c & e \end{pmatrix}$, is located between the plain mirrors [M] at distance $d/2$ from each one.

For this system, the total transformation matrix $[A, B, C, D]$ for a complete round trip is given by

$$\begin{aligned} \begin{pmatrix} A & B \\ C & D \end{pmatrix} &= \begin{pmatrix} 1 & 0 \\ 0 & -1 \end{pmatrix} \begin{pmatrix} 1 & d \\ 0 & 1 \end{pmatrix} \begin{pmatrix} 1 & 0 \\ 0 & 1 \end{pmatrix} \\ &\times \begin{pmatrix} 1 & d/2 \\ 0 & 1 \end{pmatrix} \begin{pmatrix} a & b \\ c & e \end{pmatrix} \begin{pmatrix} 1 & d/2 \\ 0 & 1 \end{pmatrix} \\ &\times \begin{pmatrix} 1 & 0 \\ 0 & 1 \end{pmatrix} \begin{pmatrix} 1 & d \\ 0 & 1 \end{pmatrix}. \end{aligned} \tag{28}$$

Matrix (29) describe a simplified ideal case whereas matrix (31) describe a general more complex and realistic case. These results will be widely used in the next three sections.

5. Tinkerbell Beams

This section presents an optical resonator that produces beams following the Tinkerbell map dynamics; these beams will be called "Tinkerbell beams". Equation (29) is the one round trip total transformation matrix of the resonator. If one does want a particular map to be reproduced by a ray in the optical resonator, each round trip described by (y_n, θ_n) , has to be considered as an iteration of the selected map. In order to obtain Tinkerbell beams, Eqs. (12) to (15) must be equated to Eq. (29), that is:

$$a + \frac{3cd}{2} = \alpha + y_n, \tag{32}$$

$$b + \frac{3d}{4}(2a + 3cd + 2e) = \beta - \theta_n, \tag{33}$$

$$c = -\gamma - 2\theta_n, \tag{34}$$

The above one round trip total transformation matrix is

$$\begin{pmatrix} a + \frac{3cd}{2} & b + \frac{3d}{4}(2a + 3cd + 2e) \\ -c & -\frac{3cd}{2} - e \end{pmatrix}. \tag{29}$$

As can be seen, the elements of this matrix depend on the elements of the map generating matrix device $[a, b, c, e]$. If one does want a specific map to be reproduced by a ray in the ring optical resonator, then each round trip a ray described by (y_n, θ_n) has to be considered as an iteration of the desired map. Then, the $ABCD$ matrix of the map system (16), (18), (27) must be equated to the total $ABCD$ matrix of the resonator (29), this in order to generate an specific map dynamics for (y_n, θ_n) .

It should be noticed that the results given by Eqs. (28) and (29) are only valid for b small ($b \approx 0$). This due to the fact that before and after the matrix element $[a, b, c, e]$ we have a propagation of $d/2$. For a general case, expression (29) has to be substituted by:

$$\begin{aligned} \begin{pmatrix} A & B \\ C & D \end{pmatrix} &= \begin{pmatrix} 1 & 0 \\ 0 & -1 \end{pmatrix} \begin{pmatrix} 1 & d \\ 0 & 1 \end{pmatrix} \begin{pmatrix} 1 & 0 \\ 0 & 1 \end{pmatrix} \\ &\times \begin{pmatrix} 1 & \frac{d-b}{2} \\ 0 & 1 \end{pmatrix} \begin{pmatrix} a & b \\ c & e \end{pmatrix} \begin{pmatrix} 1 & \frac{d-b}{2} \\ 0 & 1 \end{pmatrix} \\ &\times \begin{pmatrix} 1 & 0 \\ 0 & 1 \end{pmatrix} \begin{pmatrix} 1 & d \\ 0 & 1 \end{pmatrix} \end{aligned} \tag{30}$$

Therefore the round trip total transformation matrix is:

$$\begin{pmatrix} a - \frac{c}{2}(b - 3d) & \frac{1}{4}[b^2c - 2b(-2 + a + 3cd + e) + 3d(2a + 3cd + 2e)] \\ -c & \frac{1}{2}(bc - 3cd - 2e) \end{pmatrix} \tag{31}$$

$$e + \frac{3cd}{2} = -\delta, \tag{35}$$

Equations (32-35) define a system for the matrix elements a, b, c, e , that guarantees a Tinkerbell map behaviour for a given ray (y_n, θ_n) . These elements can be written in terms of the map parameters (α, β, γ and δ), the resonator's main parameter d and the ray state variables y_n and θ_n as:

$$a = \alpha + \frac{3}{2}\gamma d + 3d\theta_n + y_n, \tag{36}$$

$$b = \frac{1}{4}(4\beta - 6\alpha d + 6\delta d - 9\gamma d^2 - 4\theta_n - 18d^2\theta_n - 6dy_n), \tag{37}$$

$$c = -2\theta_n - \gamma, \tag{38}$$

$$e = -\delta + \frac{3}{2}d(\gamma + 2\theta_n). \tag{39}$$

The introduction of the above values for the $\begin{pmatrix} a & b \\ c & e \end{pmatrix}$ matrix in Eq. (28) enables us to obtain Eq. (16). For any

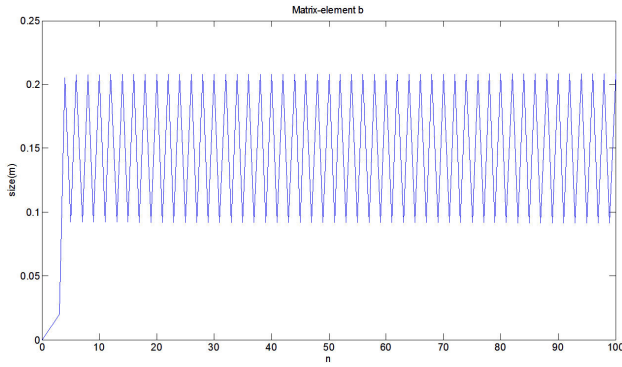


FIGURE 2. Computer calculation of the magnitude of matrix element b of the Tinkerbell map generating device for a resonator with $d = 1$ and Tinkerbell parameters $\alpha = 0, \beta = -0.6, \gamma = 0$ and $\delta = -1$ for the first 100 round trips.

transfer matrix elements A and D describe the lateral magnification while C describe the focal length, whereas the device's optical thickness is given by $B = L/n$, where L is its length and n its refractive index. From Eqs. (36-39) it must be noted that the upper elements (a and b) of the device matrix depend on both state variables (y_n and θ_n) while the lower elements (c and e) only on the state variable θ_n . The study of the stability and chaos of the Tinkerbell map in terms of its parameters is a well-known topic [22,23]. The behaviour of element b is quite interesting; Fig. 2 shows a computer calculation for the first 100 round trips of matrix element b of the Tinkerbell map generating device for a resonator of unitary length ($d = 1$) and map parameters $\alpha = 0, \beta = -0.6, \gamma = 0$ and $\delta = -1$, these parameters were found using brute force calculations and they were selected due to the matrix-element b behaviour (*i.e.* we were looking for behaviour able to be achievable in experiments). As can be seen, the optical length of the map generating device varies on each round trip in a periodic form, this would require that the physical length of the device, its refractive index -or a combination of both- change in time. The actual design of a physical Tinkerbell map generating device for a unitary ring resonator must satisfy Eqs. (36-39), to do so its elements (a, b, c and e) must vary accordingly.

5.1. Tinkerbell beams: General Case

To obtain the Eqs. (36-39) b , the thickness of the Tinkerbell generating device, has to be very small (close to zero), so the translations before and after the device can be over the same distance $d/2$. In the previous numeric simulation b takes values up to 0.2, so the general case where the map generating element b does not have to be small must be studied. As previously explained Eq. (28) must be substituted by Eq. (30).

From Eqs. (16) and (31) we obtain the following system of equations for the matrix elements a, b, c and e :

$$a - \frac{c}{2}(b - 3d) = \alpha + y_n, \tag{40}$$

$$\frac{1}{4}(b^2c - 2b(-2 + a + 3cd + e) + 3d(2a + 3cd + 2e)) = \beta - \theta_n, \tag{41}$$

$$-c = \gamma + 2\theta_n, \tag{42}$$

$$\frac{bc - 3cd - 2e}{2} = \delta. \tag{43}$$

The solution to this new system is written as:

$$a = \alpha + \frac{3}{2}\gamma d + 3d\theta_n + y_n + \frac{1}{2\gamma + 4\theta_n} \times \begin{pmatrix} \gamma(2 - \alpha + \delta - 3\gamma d - 12d\theta_n - y_n) \\ +\theta_n(4 - 2\alpha + 2\delta - 12d\theta_n - 2y_n) \\ -(-\frac{\gamma}{2} - \theta_n)\sqrt{P^2 - Q} \end{pmatrix}, \tag{44}$$

$$b = \frac{1}{\gamma + 2\theta_n} \times \begin{pmatrix} -2 + \alpha - \delta + 3\gamma d + 6d\theta_n + y_n + \frac{\sqrt{P^2 - Q}}{2} \end{pmatrix}, \tag{45}$$

$$c = -\gamma - 2\theta_n, \tag{46}$$

$$e = \delta + \frac{3}{2}\gamma d + 3d\theta_n + \frac{1}{2\gamma + 4\theta_n} \times \begin{pmatrix} \gamma(2 - \alpha + \delta - 3\gamma d - 12d\theta_n - y_n) \\ +\theta_n(4 - 2\alpha + 2\delta - 12d\theta_n - 2y_n) \\ -(-\frac{\gamma}{2} - \theta_n)\sqrt{P^2 - Q} \end{pmatrix}, \tag{47}$$

where:

$$P = 4 - 2\alpha + 2\delta - 6\gamma d - 12d\theta_n - 2y_n$$

and

$$Q = (4\gamma + 8\theta_n)(-4\beta + 6\gamma d - 6\delta d + 9\gamma d^2 + 4\theta_n + 18d^2\theta_n + 6dy_n).$$

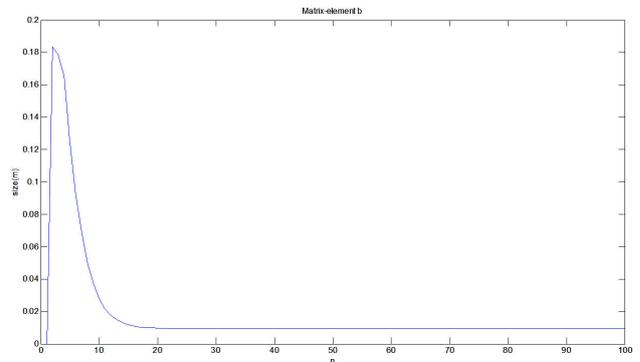


FIGURE 3. Computer calculation of the magnitude of matrix element b of the Tinkerbell map generating device for a resonator with $d = 1$ and Tinkerbell parameters $\alpha = 0.4, \beta = -0.4, \gamma = -0.3$ and $\delta = 0.225$ for the first 100 round trips.

It should be noted that if one takes into account the thickness of the map generating element, the equations complexity is substantially increased. Now only c has a simple relation with θ_n and γ , on the other hand a, b and e are dependent on both state variables, on all Tinkerbell parameters, as well as on the resonator length. When the calculation is performed for this new matrix with the following map parameters: $\alpha = 0.4, \beta = -0.4, \gamma = -0.3$ and $\delta = 0.225$, Fig. 3 is obtained. The behaviour observed in Fig. 3 for the matrix-element b can be obtained for several different parameters' combinations, as well as other dynamical regimes with a lack of relevance to our work. One can note that after a few iterations the device's optical thickness is small and constant, this should make easier a physical implementation of this device.

6. Duffing Beams

This section presents an optical resonator that produces beams following the Duffing map dynamics; these beams will be called "Duffing beams". Equation (29) is the one round trip total transformation matrix of the resonator. If one does want a particular map to be reproduced by a ray in the optical resonator, each round trip described by (y_n, θ_n) , has to be considered as an iteration of the selected map. In order to obtain Duffing beams, Eqs. (23) to (26) must be equated to Eq. (29), that is:

$$a + \frac{3cd}{2} = 0, \tag{48}$$

$$b + \frac{3d}{4} (2a + 3cd + 2e) = 1, \tag{49}$$

$$-c = -\beta, \tag{50}$$

$$-\frac{3cd}{2} - e = \alpha - \theta_n^2. \tag{51}$$

Equations (48-51) define a system for the matrix elements of a, b, c, e , enabling the generation of a Duffing map for the y_n and θ_n state variables. Its solution is:

$$a = -\frac{3\beta d}{2}, \tag{52}$$

$$b = \frac{1}{4} (4 + 6\alpha d + 9\beta d^2 - 6d\theta_n^2), \tag{53}$$

$$c = \beta, \tag{54}$$

$$e = -\alpha - \frac{3d\beta}{2} + \theta_n^2. \tag{55}$$

As can be seen these matrix elements depend on the Duffing parameters α and β as well as on the resonator main parameter d and on the state variable θ_n . These are the values which must be substituted for the $[a, b, c, e]$ matrix in Eq. (28) for the round trip matrix. As expected, the introduction of the above $[a, b, c, e]$ matrix elements in Eq. (29) produces the $ABCD$ matrix of the Duffing Map, Eq. (27). For a general $ABCD$ transfer matrix, elements A and D are related to the

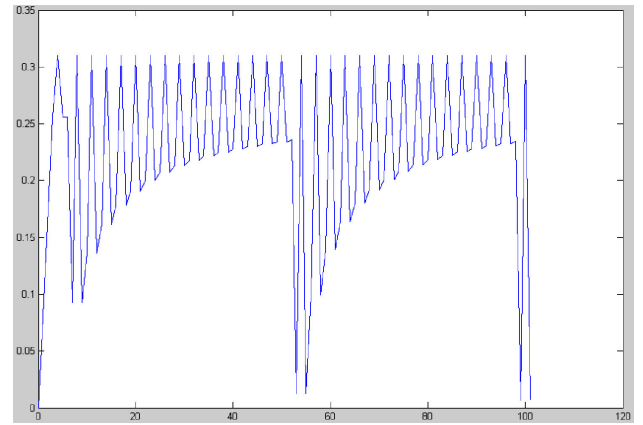


FIGURE 4. Computer calculation of the magnitude of matrix element b of the Duffing map generating device for a resonator with $d = 1$ and Duffing parameters $\alpha = 1.04$ and $\beta = -1$ for the first 100 round trips.

lateral magnification and element C to the focal length, whereas element B gives the optical length of the device. The optical thickness of the $ABCD$ is; $B = L/n$, where L is the physical length of the device and n its refractive index. From Eqs. (52-55) we may see that the A and C elements of the matrix $[a, b, c, e]$ are constants depending only on the resonator parameter d and the Duffing parameters α and β . However matrix elements B and D are dynamic ones and depend on the state variable θ_n . Of special interest is element B of the map generating matrix $[a, b, c, e]$. Figure 4 shows a computer calculation of matrix element B of the Duffing map generating device for a resonator with $d = 1$ and Duffing parameters $\alpha = 1.04$ and $\beta = -1$ for the first 100 round trips. As it is well known, depending on the α and β map parameters different dynamic states may be obtained including chaos. As can be seen the optical length of the map generating device given by the B matrix element varies on each round trip. This requires that either the physical length of the device or its refractive index, or a combination of both, changes as shown in Fig. 4. The design of a physical Duffing map generating device for this resonator must satisfy Eqs. (52-55). A physical implementation of this device is possible as long as its $ABCD$ elements vary according to these equations.

6.1. Duffing Beams: General Case

The results given by Eqs. (52-55) are valid only when the b element of the $[a, b, c, e]$ matrix is small. As can be seen from Eq. (28), the thickness of the Duffing map generating element (described by matrix $[a, b, c, e]$) must be close to zero. This because in Eq. (28) the matrix before and after the $[a, b, c, e]$ is a matrix for a $d/2$ translation which is possible only if $b = 0$ or very small. The previous numeric simulation shows that the b element takes the values of up to 0.3. Therefore one must consider a general case where the map generating element b has not the limitation of being asked to be small. For a general case, Eq. (28) must be substituted by Eq. (30) and (31). From expressions (27) and (31) we obtain

the following system of equations for the matrix elements a, b, c, e ;

$$a - \frac{c}{2}(b - 3d) = 0, \tag{56}$$

$$\frac{1}{4}(b^2c - 2b(-2 + a + 3cd + e) + 3d(2a + 3cd + 2e)) = 1, \tag{57}$$

$$-c = -\beta, \tag{58}$$

$$\frac{bc - 3cd - 2e}{2} = \alpha - \theta_n^2. \tag{59}$$

The solution to this system is given by:

$$a = \frac{2 + \alpha - \theta_n^2 + \sqrt{\alpha^2 + 4\beta(-1 + 3d) - 2\alpha(-2 + \theta_n^2) + (-2 + \theta_n^2)^2}}{2}, \tag{60}$$

$$b = \frac{2 + \alpha + 3\beta d - \theta_n^2 + \sqrt{\alpha^2 + 4\beta(-1 + 3d) - 2\alpha(-2 + \theta_n^2) + (-2 + \theta_n^2)^2}}{\beta}, \tag{61}$$

$$c = \beta, \tag{62}$$

$$e = \frac{2 - \alpha + \theta_n^2 + \sqrt{\alpha^2 + 4\beta(-1 + 3d) - 2\alpha(-2 + \theta_n^2) + (-2 + \theta_n^2)^2}}{2}. \tag{63}$$

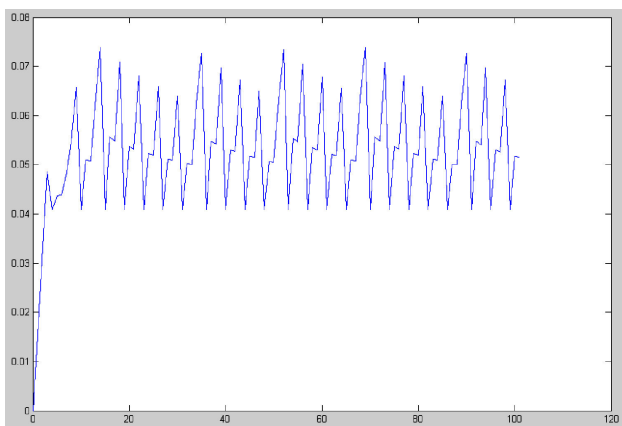


FIGURE 5. Computer calculation of the magnitude of matrix element b of the Duffing map generating device for a resonator with $d = 1$ and Duffing parameters $\alpha = 1.04$ and $\beta = -0.6$ for the first 100 round trips.

As we may see, taking into account the thickness of the map generating element device described by matrix $[a, b, c, e]$ greatly increases its complexity. Now only the C matrix element is constant, being elements A, B and D dependent on the state variable θ_n and on the Duffing parameters α and β as well as on the resonator main parameter d . Figure 5 shows a computer calculation of the matrix element B of the Duffing map generating device for a resonator with $d = 1$ and Duffing parameters $\alpha = 1.04$ and $\beta = -0.6$ for the first 100 round trips. As can be seen, the optical thickness variation of the map generating device now is rather small, which means that the length and/or refractive index variation of the map generating element is also small and favors a physical realization of this device.

7. Hénon Beams

This section presents an optical resonator that produces beams following the Hénon map dynamics; these beams will be called “Hénon beams”. Equation (29) is the one round trip total transformation matrix of the resonator. If one does want a particular map to be reproduced by a ray in the optical resonator, each round trip described by (y_n, θ_n) , has to be considered as an iteration of the selected map. In order to obtain Hénon beams, the $[A, B, C, D]$ elements of Eq. (18) must be equated to Eq. (29), that is:

$$a + \frac{3cd}{2} = \frac{1}{y_n} - \alpha y_n, \tag{64}$$

$$b + \frac{3d}{4}(2a + 3cd + 2e) = 1, \tag{65}$$

$$-c = \beta, \tag{66}$$

$$-\frac{3cd}{2} - e = 0. \tag{67}$$

The solution for the Hénon chaos matrix elements $[a, b, c, e]$, able to produce Hénon beams in terms of the Hénon Map are the following:

$$a = \frac{3\beta d}{2} + \frac{1}{y_n} - \alpha y_n, \tag{68}$$

$$b = 1 + \frac{3}{2}d \left(-\frac{1}{y_n} + \alpha y_n - \frac{3d\beta}{2} \right), \tag{69}$$

$$c = -\beta, \tag{70}$$

$$e = \frac{3d\beta}{2}. \tag{71}$$

As can be seen the matrix elements depend on the Hénon parameters α and β as well as on the resonator main parameter d and on the state variable y_n . However when analyzing the behavior of element “ b ” (Eq. (69)) we may see that there is a problem caused by the term $1/y_n$. While for the case of Tinkerbell and Duffing beams we were able to look at the behavior of the obtained “ b ” element for small values of y_n , as it is shown in figures (2-5), this is not possible for the Henon

case because small values of y_n will produce very large values for “ b ”, therefore making very difficult to obtain solutions with practical value.

7.1. Hénon Beams: General Case

In an analogous way to the two previous cases, using expression (18) and (31) we obtain for the general Hénon chaos matrix elements $[a, b, c, e]$:

$$a = \frac{-1 - 2y_n + \alpha y_n^2 + \sqrt{1 - 4y_n - 2(-2 + \alpha - 2\beta + 6\beta d)y_n^2 + 4\alpha y_n^3 + \alpha^2 y_n^4}}{2y_n}, \tag{72}$$

$$b = \frac{1 + (-2 + 3\beta d)y_n - \alpha y_n^2 + \sqrt{1 - 4y_n - 2(-2 + \alpha - 2\beta + 6\beta d)y_n^2 + 4\alpha y_n^3 + \alpha^2 y_n^4}}{2y_n}, \tag{73}$$

$$c = -\beta, \tag{74}$$

$$e = \frac{-1 + 2y_n + \alpha y_n^2 - \sqrt{1 - 4y_n - 2(-2 + \alpha - 2\beta + 6\beta d)y_n^2 + 4\alpha y_n^3 + \alpha^2 y_n^4}}{2y_n}. \tag{75}$$

8. A practical map generating device

As we have seen, in order to generate an $ABCD$ matrix system such as (11) it is essential to introduce an intra-cavity element which will be responsible for taking into account the hysteresis and non-linearity of the dynamic system. The intra-cavity map generating device is described by a 2×2 matrix, where its elements are given by Eqs. 10. The equations describing the intracavity element are:

$$y_{\text{output}} = ay_{\text{input}} + b\theta_{\text{input}}, \tag{76}$$

$$\theta_{\text{output}} = cy_{\text{input}} + e\theta_{\text{input}}. \tag{77}$$

The practical implementation of an intra-cavity element is technically a complex task due to the fact that the actual intra-cavity matrix is a dynamic one, its value depends not only on the map constants but also on the previous round-trip y_n and θ_n values [30]. In particular it is required for the intra-cavity element a system able to detect and measure the position and angle of incidence of the input beam parameters, *i.e.* y_{input} and θ_{input} , this information should be optically or electronically process (according to Eqs. 18-21) in order to produce and generate the required output beam with new parameters *i.e.* y_{output} and θ_{output} . A general intra-cavity element does not yet exist.

The measurement of the impinging angle of a light beam can be implemented by several techniques, such as the use of collimators or interferometers. However, when the spatial coordinates are also of interest, as in this case, there is not a straightforward solution. A possible solution is the use of a matrix of photosensors mounted on a PZT-driven stage. As shown in Fig. 6, a projected spot results from the projection of the beam onto the plane of the photosensors. The angle can be obtained by measuring the spatial coordinates of the spot for two different positions. To obtain measurement speeds on

the order of milliseconds it is necessary that the PZT stage be driven at relatively high speeds, *e.g.* the M-663 stage from Physik Instruments can reach displacement speeds of up to 400 mm/s (travel range of 19 mm with 100 nm resolution). A matrix of photosensor such as that offered by Centronic, *i.e.*, 12×12 elements, each element of 1.4×1.4 mm, can be used as a first approximation. In this case, by considering the travel range of the stage, the maximum transverse displacement of the beam spot, at the sensor plane, would be 3 pix, where one pixel corresponds to one sensor element; for this computation it was assumed that ray angles are less than 15° . This arrangement would yield measurements with low accuracy. To increase the accuracy of the measurement, the separation between neighboring elements should be decreased.

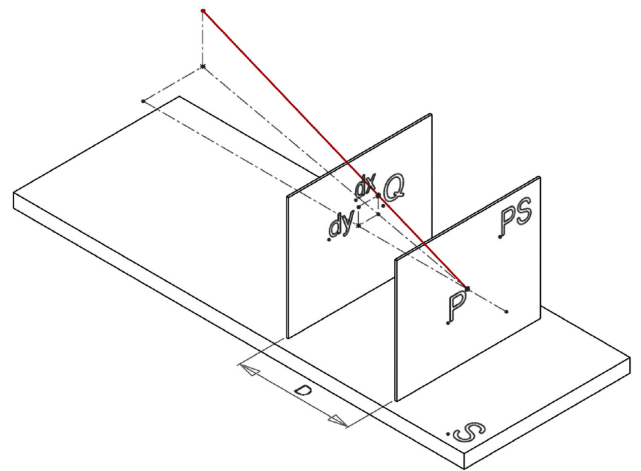


FIGURE 6. A photosensor array (PS) is translated by a PZT stage (S) a distance D . This produces a displacement of the beam spot from P to Q , dx and dy . The incidence angles of the ray are given by $\theta_x = \tan^{-1}(dx/D)$ and $\theta_y = \tan^{-1}(dy/D)$. The light beam is indicated by the red line.

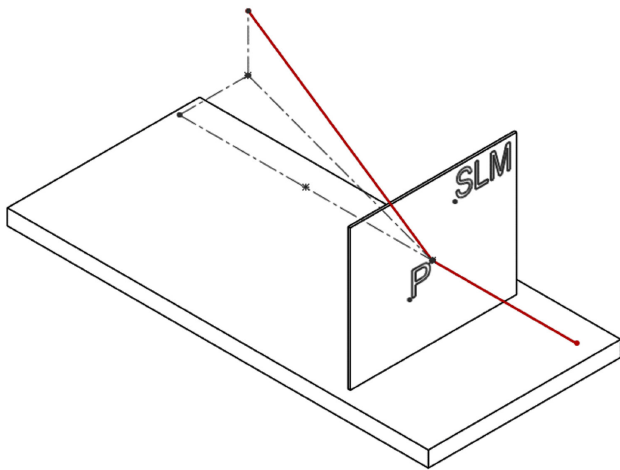


FIGURE 7. Beam steering by a SLM. The beam impinges on the SLM from the right.

This can be achieved by using a camera sensor, where the pitch may be as small as $4 \mu\text{m}$ at the maximum angle, the distance between the two positions of the beam spot can be as large as hundreds of pixels. However, in this case the complexity of the arrangement is increased.

On the other hand beam steering may be done by non-mechanical array devices, which provide high-speed pointing, see Fig. 7. Among these types of devices we can mention those based on liquid-crystal displays (spatial light modulators, SLM) and those on microelectromechanical systems (MEMS). In the formers, the phase of each element of the matrix is changed by application of a low-voltage signal. In the devices based on MEMS, each element of the array consists of a micromirror, which generates tilt to steer the beam. Steering time is on the order of milliseconds.

9. Conclusions

This article presents a pedagogical description of the application of non-constant ABCD matrix in the description of

ring optical phase conjugated resonators. It is shown how the introduction of a particular map generating device in a ring optical phase-conjugated resonator can generate beams with the behavior of a specific two dimensional map. In this way beams that behave according to the Tinkerbell, Duffing or Henon Maps which we call “Tinkerbell, Duffing or Henon Beams”, are obtained. In particular, this article shows how Tinkerbell beams can be produced if a particular device is introduced in a ring optical phase-conjugated resonator. The difference equations of the Tinkerbell map are explicitly introduced in an ABCD transfer matrix to control the beams behaviour. The matrix elements a , b , c and e of a map generating device are found in terms of the map parameters (α , β , γ and δ), the state variables (y_n and θ_n) and the resonator length. The mathematical characteristics of an optical device inside an optical resonator capable to produce Tinkerbell beams are found. In the general case a device with fixed size was obtained, opening the possibility of a continuance of this work; that is the actual building of an optical device with these a , b , c and d matrix elements according to the description given and the experimental observation of Tinkerbell beams. Also, it is explicitly shown how the difference equations of the Duffing map can be used to describe the dynamic behavior of what we call Duffing beams *i.e.* beams that behave according to the Duffing map. The matrix elements a , b , c , e of a map generating device are found in terms of α and β , the Duffing parameters, the state variable θ_n and the resonator parameter d . Finally it is shown that the difference equations of the Hénon map can be used to describe the dynamical behavior of Hénon beams. The matrix elements a , b , c , e of a chaos generating device are found in terms of α and β the Hénon parameters, and d the resonator parameter.

A challenge for future research is in the practical implementation of this work since it would be very interesting to build an actual optical device with the required $[a, b, c, e]$ matrix elements and realize the experimental observation of Tinkerbell, Duffing and Hénon Beams.

1. G.S. He, *Prog. in Quantum Electronics* **26** (2002) 131-191
2. H.-J. Eichler, R. Menzel, and D. Schumann, *Appl. Opt.*, **31** (1992) 5038-5043
3. M. O'Connor, V. Devrelis, and J. Munch, in *Proc. Int. Conf. on Lasers'95* (1995) 500-504
4. M. Ostermeyer, A. Heuer, V. Watermann, and R. Menzel in *Int. Quantum Electronics Conf.* OSA Technical Digest Series (Optical Society of America, Washington, DC, 1996), 259
5. I.M. Bel'dyugin, M.G. Galushkin, and E.M. Zemskov *Kvantovaya Elektron.* **11** (1984) 887 [*Sov. J. Quantum Electron.* **14** (1984) 602; Bepalov V.I. and Betin A.A. *Izv. Akad. Nauk SSSR., Ser. Fiz.* **53** (1989) 1496.
6. V.V. Yarovoi, A.V. Kirsanov, *Quantum Electronics* **32** (2002) 697-702.
7. M.J. Damzen, V.I. Vlad, V. Babin, and A. Mocofanescu, *Stimulated Brillouin Scattering: Fundamentals and Applications*, Institute of Physics, Bristol (2003)
8. D. A. Rockwell, *IEEE Journal of Quantum Electronics* **24** (1988) 1124-1140
9. Dämmig, M., Zinner, G., Mitschke, F., Welling, H. *Stimulated, Physical Review A*, **48** (1993) 3301-3309
10. P.J. Soan, M.J. Damzen, V. Aboites and M.H.R. Hutchinson, *Opt. Lett.* **19** (1994) 783
11. A.D. Case, P.J. Soan, M.J. Damzen and M.H.R. Hutchinson, *J. Opt. Soc. Am. B* **9** (1992) 374
12. B. Barrientos, V. Aboites, and M. Damzen, Temporal dynamics of a ring dye laser with a stimulated Brillouin scattering mirror, *Applied Optics*, **35** (1996) 5386-5391

13. E. Rosas, V. Aboites, M.J. Damzen, *Optics Communications* **174** (2000) 243-247
14. V. Aboites, *Int. J. of Pure and Applied Mathematics*, **36** (2007) 345-352.
15. V. Aboites and M. Wilson, *Int. J. of Pure and Applied Mathematics* **54** (2009) 429-435.
16. V. Aboites, A.N. Pisarchik, A. Kiryanov, X. Gomez-Mont, *Opt. Comm.* **283** (2010) 3328-3333
17. V. Aboites, Y. Barmenkov, A. Kir'yanov, M. Wilson, *Optical Devices* Chapter XX, *Optical Resonators and Dynamic Maps*, Ed. Intech, (In Press)
18. A. Gerrard and J.M. Burch, *Introduction to Matrix Methods in Optics* (Dover Publications Inc., New York 1994).
19. Y. Hisakado, H. Kikuchi, T. Nagamura, and T. Kajiyama, *Advanced Materials* **17** (2005) 96-97
20. A.V. Kir'yanov, V. Aboites and N.N. Ilichev, *JOSA B* **17** (2000) 11-17
21. I.D. Mayergoyz and G. Bertotti, *The Science of Hysteresis*, (Academic Press, New York 2005).
22. http://en.wikipedia.org/wiki/List_of_chaotic_maps
23. R.L. Davidchack, Y.C. Lai, A.Klebanoff, E.M. Bollt, *Physics Letters A*, **287** (2001) 99-104
24. P.E. McSharry, P.R.C. Ruffino, *Dynamical Systems* **18** (2003) 191-200
25. E. Eschenazi, H.G. Solari, and R. Gilmore, *Phys. Rev. A* **39** (1989) 2609.
26. M. Hénon, *Commun. Math. Phys.* **50** (1976) 69.
27. R.L. Devaney, *An Introduction to Chaotic Dynamical Systems*, (Addison-Wesley, Redwood City 1989).
28. L.M. Saha and R. Tehri, *Int. J. of Appl. Math and Mech.* **6** (2010) 86-93
29. C. Murakami, W. Murakami, K. Hirose and W.H. Ichikawa, *Chaos, Solitons & Fractals* **16** (2003) 233-244
30. V. Aboites, Y. Barmenkov, A. Kiryanov, M. Wilson, *Results in Physics* **2** (2012) 216-220.